CHAPTER 10

HILBERT SPECTRA OF NONLINEAR OCEAN WAVES

Paul A. Hwang, Norden E. Huang, David W. Wang and James M. Kaihatu

The Hilbert–Huang transform (HHT) analysis interprets wave nonlinearity in terms of frequency modulation instead of harmonic generation. The resulting spectrum contains much higher spectral energy at low frequency and sharper drop off at high frequency in comparison with the spectra derived from Fourier-based analysis methods. The high energy level in the low-frequency components of the Hilbert spectrum seems to be consistent with the rich group structure apparent in typical ocean-wave records. For wind-generated waves, the spectral level of the Fourier spectrum is about two orders of magnitude smaller than that of the Hilbert spectrum at the first subharmonic of the peak frequency. The mean frequency of the Fourier spectrm is 20% higher than that of the Hilbert spectrum. Furthermore, the frequency of the wave groups is also more likely to be properly identified in the Hilbert spectrum than in the Fourier spectrum. The implications for ocean engineering and air-sea interaction are discussed.

10.1. Introduction

Fourier-based spectral analysis methods have been widely used for studying random waves. One major weakness of these methods is the assumption of linear superposition of wave components. As a result, the energy of a nonlinear wave spreads into many harmonics, which are phase-coupled via the nonlinear dynamics inherent in ocean waves. In addition to the nonlinearity issue, Fourier spectral analysis should, strictly speaking, be used for periodic and stationary processes only, but wave propagation in the ocean is certainly neither stationary nor periodic.

Recently, Huang and his colleagues developed a new analysis technique, the HHT. Through analytical examples, they demonstrated the superior frequency and temporal resolutions of the HHT for analyzing nonstationary and nonlinear signals (e.g., Huang et al. 1998, 1999). A brief description of the HHT analysis technique is presented in section 10.2. Using this analysis, the physical interpretation of nonlinearity is frequency modulation, which is fundamentally different from the commonly accepted concept associating nonlinearity with harmonic generation. Huang et al. argued that harmonic generation is caused by the perturbation method used in solving the nonlinear equation governing the physical processes; thus, the harmonics are produced by the mathematical tools used for the solution rather than being a true physical phenomenon.

In section 10.3, we investigate the HHT technique for ocean-wave analysis. The spectrum of wind-generated waves is presented as a case study. The Hilbert spectrum is compared with that obtained by using the Fourier-based techniques [wavelet and fast Fourier transform (FFT) algorithms]. The wavelet technique is based on Fourier spectral analysis but with adjustable frequency-dependent window functions, the mother wavelets, to provide temporal/spatial resolution for nonstationary signals (e.g., Shen and Mei 1993; Shen et al. 1994; Liu 2000; Massel 2001). As expected, the Fourier-based analysis interprets wave nonlinearity in terms of harmonic generation; thus, the spectral energy leaks into the higher-frequency components. The HHT interprets wave nonlinearity as frequency modulation, and the spectral energy remains near the base frequencies. As a result, these two sets of spectra have significantly different spectral characteristics.

The implications of these differences for ocean-wave spectra for ocean engineering applications and air-sea interaction processes, such as the characteristic frequency of the forcing waves and other statistical properties and the group structure of a wave field, are discussed in section 10.4. A summary is given in section 10.5.

10.2. The Hilbert–Huang spectral analysis

The Hilbert transformation was first used for water-wave analysis in the 1980s (e.g., Melville 1983; Bitner-Gregersen and Gran 1983; Hwang et al. 1989). A main application of the Hilbert analysis is to derive the local wavenumber in a spatial series or the instantaneous frequency in a time series. To use the Hilbert transformation, the proper preprocessing of the signal is critical. Large errors in the computed local frequency or wavenumber can occur when small wavelets are riding on longer waves or when a sharp change in the frequency occurs in the wave signal. A quantitative illustration of the riding wave problem has been discussed in greater detail by Huang et al. (1998) and sharp changes in the frequencies of oscillations by Guillaume (2002) and will not be repeated here. The common approach in the past to alleviate such problems was to apply a low-pass filter to the signal prior to the Hilbert transformation. The determination of the low-pass frequency is somewhat subjective, and the signals removed may contain the information of nonlinearity, which is frequently the feature to be studied. Furthermore, a simple low-pass operation may not eliminate the riding wave problem.

The key ingredient in the HHT is empirical mode decomposition (EMD) designed to reposition the riding waves at the mean water level. Huang et al. (1998, 1999) have extensively discussed EMD. The main idea is to find the trend that can represent the mean local average so that riding waves can be identified. The EMD method uses the point-by-point average of the signal envelopes for the local mean. The difference between the original signal and the local mean represents a mode of the signal. The local mean may also contain riding waves, and the mode decomposition process continues until no riding waves exist in the local mean signal. The process is called "sifting" by Huang et al. (1998). From experience, even for very complicated

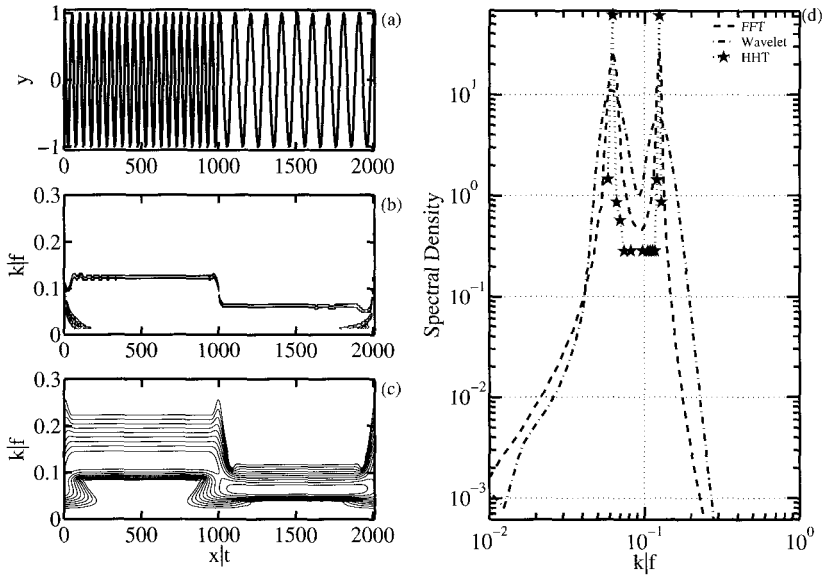

Figure 10.1: (a) Simple sinusoidal oscillations with the frequency or wavenumber of the first half double that of the second half, (b) the computed Hilbert spectrum, (c) the computed wavelet spectrum, and (d) a comparison of the spatially or temporally averaged spectra computed by the FFT, wavelet and HHT methods. The frequency (wavenumber) is normalized by the Nyquist value.

random signals, a time series can usually be decomposed into a relatively small number of modes, $M < \log_2(N)$, where M denotes the number of modes and N is the number of data points. Each mode is free of riding waves; thus, the Hilbert transformation yields the accurate local frequency of the mode. The spectrum of the original signal can be obtained by the sum of the Hilbert spectra of all modes. Extensive tests have been carried out by Huang et al. (1998, 1999). Here, we present three cases to illustrate the superior resolutions of the Hilbert spectrum.

Case 1 is an example of the ideal sinusoidal oscillations of constant amplitude. The frequency of the first half of the signal is twice that of the second half (Fig. 10.1a). The spectra computed by the HHT and wavelet techniques are displayed in Figs. 10.1b and 10.1c, respectively. The Hilbert spectrum yields very precise frequency resolution and also high temporal resolution in identifying the sudden change of signal frequency at about the half-point of the time series. In comparison, the wavelet spectrum has only a mediocre temporal resolution of the frequency change. A serious leakage problem also occurs and the spectral energy of the simple oscillations spreads over a broad frequency range. Unless specified otherwise, the spectral contours plotted in the figures presented in this chapter are 3-dB (a factor of two) apart and cover a 30-dB range. For the example given in Fig. 10.1c, the 3-dB contour near the spectral peak extends to between 0.8 and 1.2 times of the spectral peak frequency for the wavelet spectrum. In contrast, the Hilbert spectral energy is pretty much contained at the two spectral peak frequencies, and the

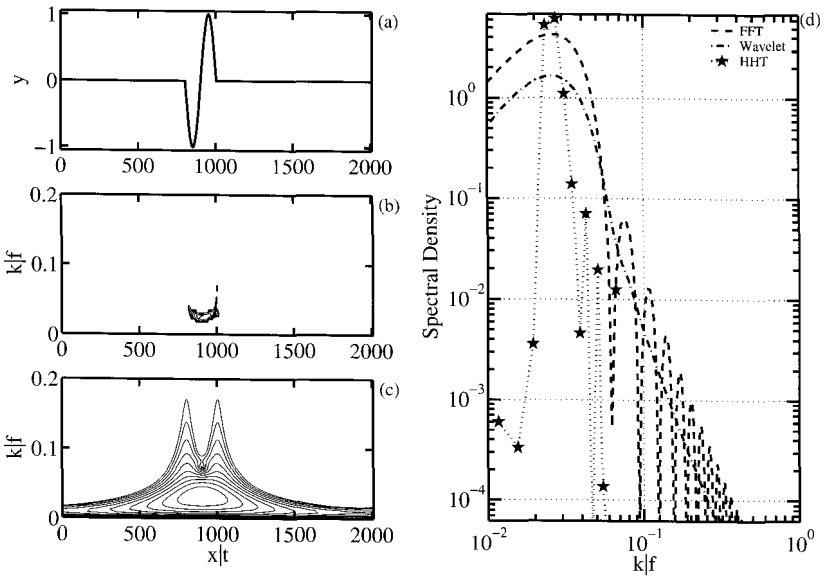

Figure 10.2: Same as Fig. 10.1 but for a transient sinusoidal wave of one cycle.

spectral density of the next frequency bin is at least 10 dB down, as estimated by averaging the marginal spectrum over the whole time sequence (Fig. 10.1d). The spectral peak discrimination power can be quantified by the ratio between the spectral peaks and the neighboring spectral valleys. For the HHT, this number is 23 dB, the FFT analysis gives 16 dB, and wavelet 8 dB. Also noticeable in Fig. 10.1d is the unequal spectral densities at the two peaks of the wavelet spectrum, caused by the application of frequency-dependent windows in the wavelet analysis. The spectral density at the second-frequency component is only about 60 % of the spectral density at the first-frequency component.

Case 2 is a single cycle sinusoidal oscillation occurring at the middle of the otherwise quiescent signal stream (Fig. 10.2a). The period of a single cycle is 32 s. The precise temporal resolution of the HHT method is clearly demonstrated by the sharp rise and fall of the Hilbert spectrum coincident with the transient signal, as illustrated in Fig. 10.2b. By comparison, the wavelet spectrum is much more smeared both in the frequency and temporal resolutions (Fig. 10.2c). The marginal spectrum derived from the analysis shows a much sharper frequency definition of the single oscillating cycle as compared to that of the wavelet and Fourier spectra (Fig. 10.2d).

Case 3 is a sinusoidal function with periodically oscillating frequencies (Fig. 10.3a)

$$y(t) = a \sin[\omega t + \epsilon \sin(\omega t)] \,. \tag{10.1}$$

This equation is the exact solution for the nonlinear differential equation (Huang

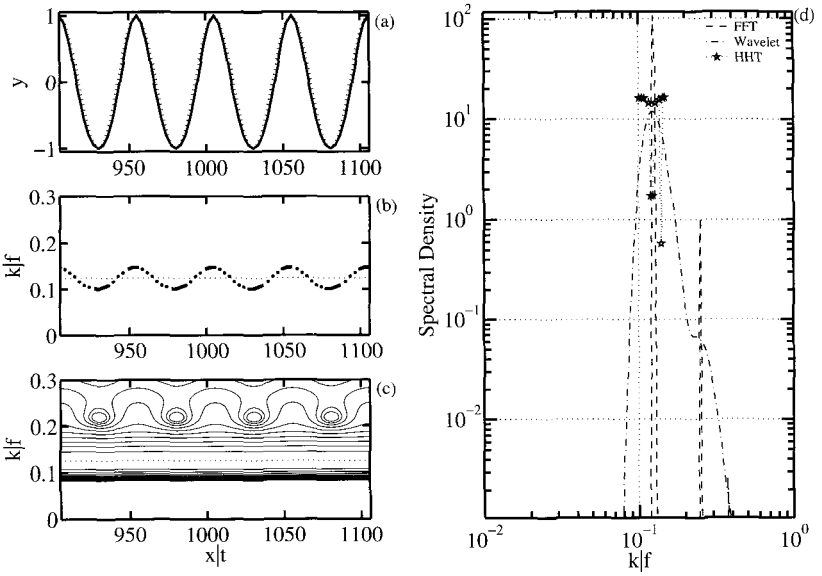

Figure 10.3: Same as Fig. 10.1 but for a signal with modulated frequency, $y(t) = a\cos[\omega t + \epsilon\sin(\omega t)]$. The unmodulated mean frequency is shown by the dotted lines in (b) and (c) for reference.

et al. 1998)

$$\frac{d^2y}{dt^2} + [\omega + \epsilon\omega\cos(\omega t)]^2 y - \sqrt{1-y^2}\epsilon\omega^2\sin(\omega t) = 0\,. \tag{10.2}$$

If the perturbation method is used to solve (10.2), the solution to the first order of ϵ is

$$y_1(t) = \cos(\omega t) - \epsilon\sin^2(\omega t) = \cos(\omega t) - \epsilon\left\{\tfrac{1}{2}\left[1 - \cos(2\omega t)\right]\right\}\,. \tag{10.3}$$

The Hilbert spectrum (Fig. 10.3b) correctly reveals the nature of the oscillatory frequencies of the exact solution (10.1). In contrast, the wavelet spectrum (Fig. 10.3c) shows a dominant component at the base frequency and periodic oscillations of the second-harmonic component. In the marginal spectrum (Fig. 10.3d), the HHT analysis shows that the spectral energy is confined in the narrow frequency band surrounding the base frequency, which reflects the nature of the frequency modulation of the nonlinear system (10.2). Both FFT and wavelet analyses spread the spectral energy into higher frequencies as a result of harmonic generation by the Fourier decomposition of a nonlinear signal. The Fourier decomposition turns out to be a perfect match for representing the perturbation solutions such as (10.3). In this example, we have chosen $\epsilon = \frac{1}{5}$, so the spectral density of the second harmonic is $\frac{1}{100}$ of the primary component, which is accurately reproduced by the Fourier spectrum. The wavelet spectrum under-predicts the magnitude of the second harmonic by about 40%, similar to the results in Case 1 (Fig. 10.1d).

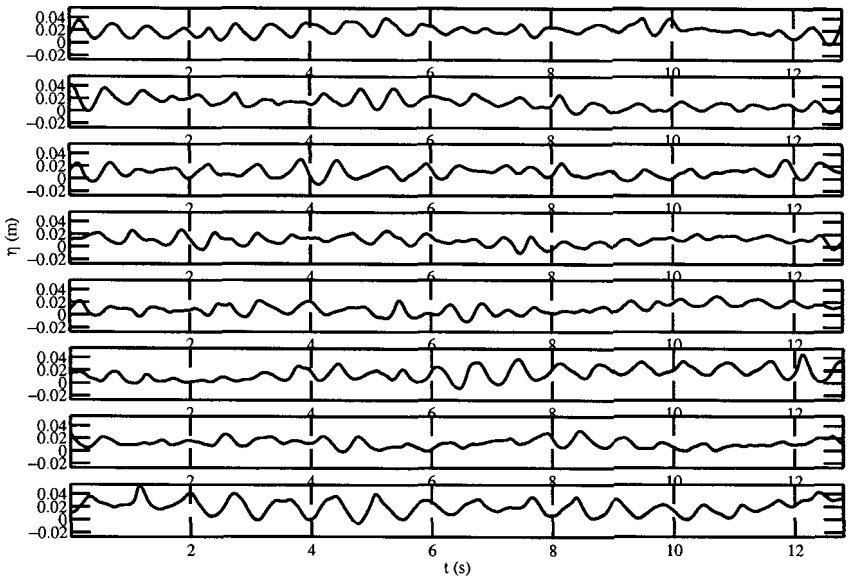

Figure 10.4: Examples of the time series of wind-generated waves used for spectral comparison. The average wind speed is about 5 m s^{-1}. The data are measured by a fast response wire gauge sampled at 50 Hz.

The three examples shown above illustrate the excellent temporal (spatial) and frequency (wavenumber) resolution of the HHT method for processing nonlinear and nonstationary signals. Many more demonstration cases are presented by Huang et al. (1998, 1999).

10.3. Spectrum of wind-generated waves

Here, we investigate the impact on the wind wave spectral functions by using different the spectral analysis techniques described in section 10.2. The wave record is acquired by using a fast-response wire gauge (Chapman and Monaldo 1991; Hwang and Wang 2004) during a test deployment in a canal (approximately 100 m wide and 400 m long). The data are sampled at 50 Hz, and the wind condition is light and variable with a range between 0 and 5 m s^{-1}. Figure 10.4 displays examples of the wave record showing the typical quasi-random time series of wind waves rich with group structure. The peak wave period is somewhat longer than 0.6 s, and one expects considerably lower frequency energy associated with the wave groups. Most groups have between 3 and 10 carrier waves.

Wave spectra are calculated by using the three methods using 20 segments of the wave record. Each segment contains 640 data points (12.8 s). For the Fourier spectrum, the mean of the 20 raw spectra is further running-averaged across nine frequency bins, resulting in the final spectrum with 360 degrees of freedom. For the Hilbert and wavelet spectra, each data segment produces a temporal variation

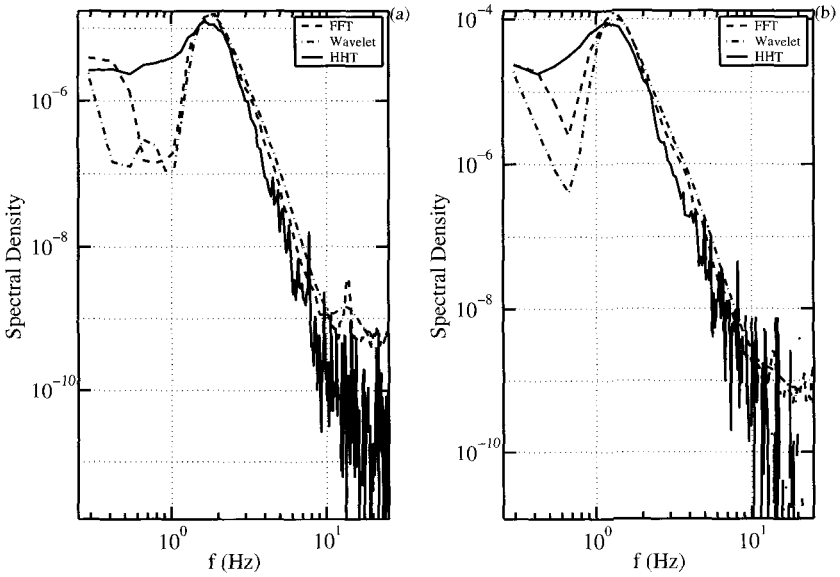

Figure 10.5: Spectra of wind-generated waves. The average wind speed is (a) 2 m s^{-1} and (b) 5 m s^{-1}.

of the wave spectrum. The average over time gives the marginal (one-dimensional) spectrum. The procedure is repeated for the 20 segments to obtain the final average Hilbert and wavelet frequency spectra. Figure 10.5 compares the spectra derived from these three different processing procedures. The similarities and differences of the spectral properties are described below.

The peak frequencies of the three spectra are close to 1.9 Hz for average wind speed $U = 2$ m s^{-1} (Fig. 10.5a) and 1.4 Hz at $U = 5$ m s^{-1} (Fig. 10.5b). A secondary peak near the frequency component with minimum phase speed, $f_m = 13.6$ Hz, is very prominent in the Fourier spectrum. The secondary peak is still discernable in the wavelet spectrum, but is buried in the noise of the Hilbert spectrum.

Overall, the wavelet spectrum represents a smoothed version of the Fourier spectrum. The two Fourier-based spectra produce essentially similar results. The differences between the two spectra can be attributed to the degree of freedom, which is considerably higher in the wavelet analysis through the multiple windowing procedure.

The Hilbert spectrum differs from the other two Fourier-based spectra in two main areas. The spectral density at the low-frequency portion is considerably higher in the Hilbert spectra, but near the peak and at higher frequencies, the reverse is true. As we have emphasized in the last section, this result is expected because of the HHT's and the Fourier-based methods' different intrepretations of wave nonlinearity. Fourier-based techniques always decompose a nonlinear wave into its base frequency and higher harmonics; therefore, some spectral energy in the higher fre-

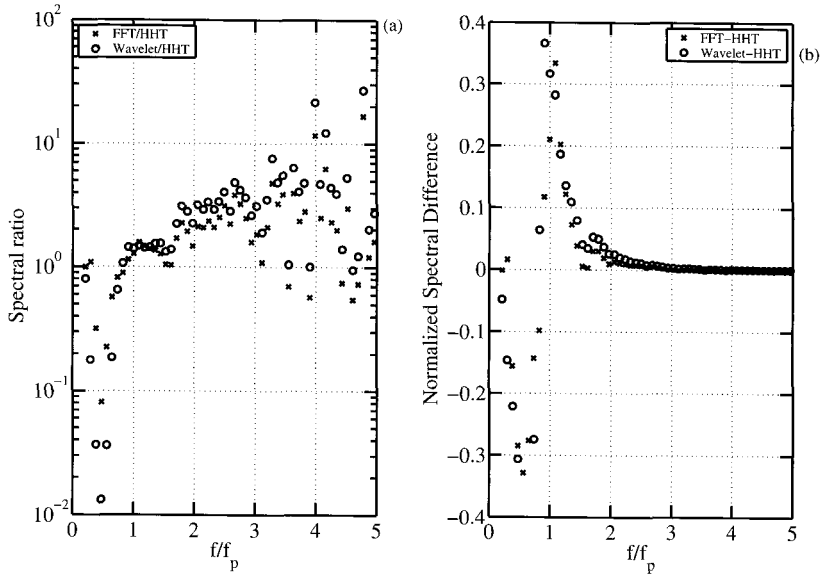

Figure 10.6: (a) The ratios of wavelet and Fourier spectra normalized by the Hilbert spectrum. (b) The difference spectra normalized by the Hilbert peak spectral density. The average wind speed is 5 m s^{-1}. Similar results are found for 2 m s^{-1} wind condition.

quencies is leaked from their lower frequency subharmonics. There are higher-order spectral-processing methods, such as bispectrum and trispectrum, designed to restore the nonlinearity-contributed high-frequency spectral energy to the base frequency. It is fair to say that Fourier-based methods always overestimate the spectral level at frequencies higher than the spectral peak. The HHT interprets wave nonlinearity in terms of frequency modulation, and the spectral energy of a nonlinear wave remains at the neighborhood of the base frequency (see also Fig. 10.3d).

Figure 10.6a shows the ratio of the spectral densities, S_F/S_H and S_w/S_H, where subscripts F, H, and w denote the FFT, HHT, and wavelet, respectively. If we use the Hilbert spectrum as a reference, the spectral density derived from Fourier-based analysis is in general much lower (by a factor of about 80 at its minimal point) at low frequencies and much higher (by about a factor of 10) at high frequencies. We also processed the spectral difference normalized by the peak spectral density, $(S_F - S_H)/S_H(f_p)$ and $(S_w - S_H)/S_H(f_p)$. The results are shown in Fig. 10.6b. Significant differences in the spectral properties are obvious in the frequency region lower than the second harmonic of the peak frequency.

These differences in the frequency distribution of wave energy certainly impact ocean engineering designs. For example, the mean frequency as defined by the normalized first moment of the wave spectrum,

$$f_1 = \int fS(f)\,df \Big/ \int S(f)\,df\,, \tag{10.4}$$

is 13% lower in the Hilbert spectrum than that in the Fourier spectrum, and 21% lower than that in the wavelet spectrum for the examples shown in Fig. 10.5. These results clearly show that the Hilbert spectral level is considerably higher than the Fourier-based spectra in the lower frequency region. In the higher frequency portion, the Hilbert spectrum shows a steeper dropoff than the Fourier-based spectra. These differences in the wave spectral properties affect many engineering applications such as the frequency response of marine structures. Based on the interpretation of nonlinearity as frequency modulation, the mean frequency of the ocean-wave spectrum is about 1.2 times lower than that given by Fourier analysis.

10.4. Statistical properties and group structure

As a result of the spectral downshift in the Hilbert spectrum in comparison with the Fourier-based spectra as shown in Fig. 10.5, the characteristics of the spectral bandwidth may differ when different processing methods are used. The investigation of the spectral bandwidth is of some interest because it is closely related to the statistical properties of ocean waves. The dimensionless frequency bandwidth of a wave spectrum is defined (Longuet-Higgins 1952, 1980; Huang et al. 1983) by

$$\nu^2 = \frac{m_0 m_2 - m_1^2}{m_1^2} = \frac{f_2^2 - f_1^2}{f_1^2}, \tag{10.5}$$

where m_i is the ith moment of the wave spectrum, and f_i is the characteristic frequency defined by the ith moment of the wave spectrum. As we commented earlier, wave nonlinearity results in harmonic generation in Fourier-based processing; therefore, for a wind wave spectrum, $f_2 > f_1$ is always true. With the Hilbert spectrum, the nonlinearity is seen as a frequency modulation near the spectral peak. It is less clear whether $f_2 > f_1$ would hold true. We apply the HHT and wavelet analysis to two wind wave data sets with nominal wind speeds of 2 and 5 m s^{-1}. The results are displayed in Figs. 10.7a and 10.7b. If we use either processing method, $f_2 > f_1$ for both cases, and the ratios of f_1/f_2 from both processing methods are quite compatible. The calculated ν^2 from the two methods and their ratio are shown in Figs. 10.7c and 10.7d, and also show good agreement. In Figs. 10.7c and 10.7d, the bandwidth computed from the ensemble-averaged spectra from the FFT, wavelet and HHT are also displayed. The results from the HHT and FFT are almost identical. This finding suggests that the study of the statistical properties of ocean waves using wave spectral functions is probably not affected by using the Hilbert spectral technique.

As displayed in Fig. 10.4, ocean waves in nature almost always exhibit a group structure, strongly suggesting the presence of energy in the low-frequency components. The Hilbert transform has been widely used in the investigation of the envelope and group structure of surface waves (Melville 1983; Bitner-Gregersen and Gran 1983; Hwang et al. 1989; Veltchva 2002; Veltchva et al. 2003).

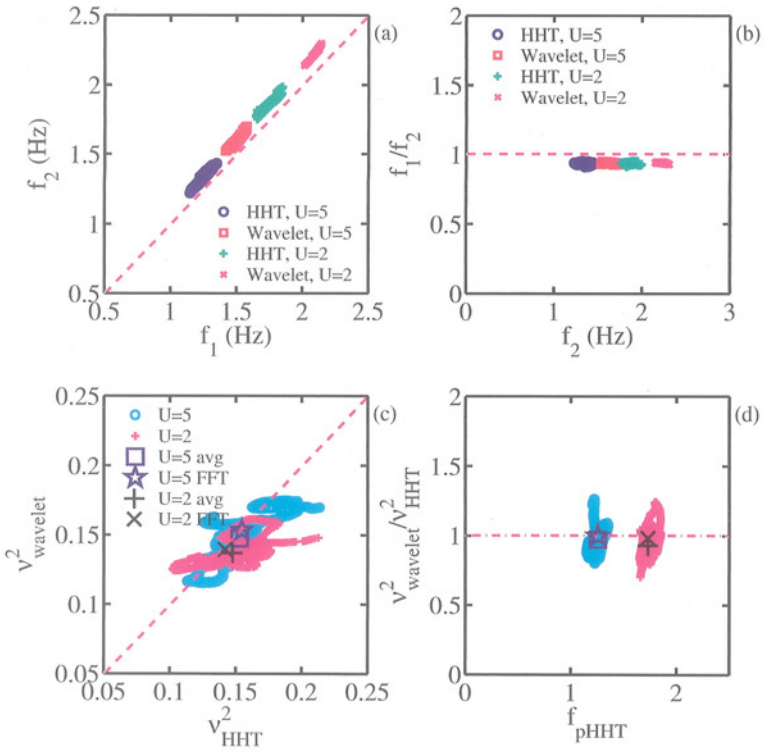

Figure 10.7: (a) Comparison of the characteristic frequencies f_2 and f_1 derived from the HHT and wavelet analyses, (b) ratio f_1/f_2 plotted as a function of f_2, (c) dimensionless bandwidth ν^2 derived from the HHT and wavelet analyses, (d) ratio $\nu^2_{wavelet}/\nu^2_{HHT}$ plotted as a function of f_p, where f_p is the spectral peak frequency.

The low-frequency energy can be produced, for example, by the interaction of two wave components with a small frequency difference (frequency beating). When FFT-based techniques are used, such low-frequency energy cannot be easily detected. As an illustrative example, let us examine the following simple case of amplitude modulation (AM) of carrier waves with an angular frequency of ω_0,

$$y = \cos(\delta\omega\, t)\cos(\omega_0 t) = \cos\left[\left(\omega_0 + \frac{\delta\omega}{2}\right)t\right] + \cos\left[\left(\omega_0 - \frac{\delta\omega}{2}\right)t\right]. \qquad (10.6)$$

Because of the mathematical equivalence of the two expressions in the right side of (10.6), Fourier decomposition interprets the signal as two sinusoidal oscillations of equal amplitude with frequencies at $\omega_0 + \delta\omega/2$ and $\omega_0 - \delta\omega/2$. The HHT, with its mode decomposition nature, will identify the low-frequency component. Figure 10.8a shows the AM time series with a normalized (by the Nyquist value) carried wave frequency of 0.4 and a modulation frequency one tenth of the carrier frequency. The spectra produced by three difference analysis techniques are shown

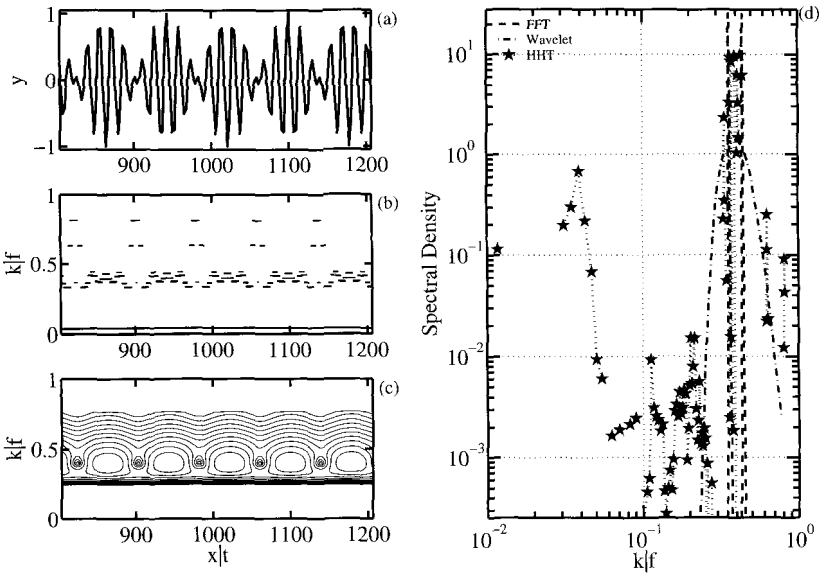

Figure 10.8: (a) Time/space series of an amplitude modulation signal showing the group structure. (b) The temporal/spatial Hilbert spectrum, (c) the temporal/spatial wavelet spectrum, and (d) the average Hilbert, wavelet, and Fourier spectra. The carrier period is $5\Delta t$, and the modulation period is $50\Delta t$, where Δt is the sampling time interval.

in Fig. 10.8d. The FFT processing produces two spectral components at 0.36 and 0.44. The small frequency difference is usually difficult for the wavelet processing to distinguish because of the relatively short dynamic windows used. In comparison, the HHT is able to identify both the carrier and the modulation frequency components at the correct frequencies of 0.4 and 0.04. The Hilbert spectrum, however, also contains energy at subharmonic and superharmonic frequencies, although the energy levels are relatively small: about -20 dB or smaller in comparison with the peak energy level. These sub- and super-harmonic components occur at the nodal points of the time series (Fig. 10.8b) and suggest that they are the results of a low signal-to-noise ratio.

The ability of the HHT to identify the modulation (group) frequency, as mentioned earlier, is attributed to the nature of mode decomposition. Figure 10.9 plots the time series of the original signal and the decomposed empirical modes. The modulation frequency component shows up in mode 4 for the present example. From our experience, artificial subharmonics usually occur in the presence of groupiness in the signal. The problem of artificial subharmonic components is especially serious when the group structure is weak. For example, Fig. 10.10 plots a case in which the modulation frequency is 5 times lower than the carrier frequency. The spectral densities at the frequency components between the carrier and modulation frequencies are comparable to that at the modulation frequency (Fig. 10.10d). Based on our experience, it is not unusual that the modulation frequency component disap-

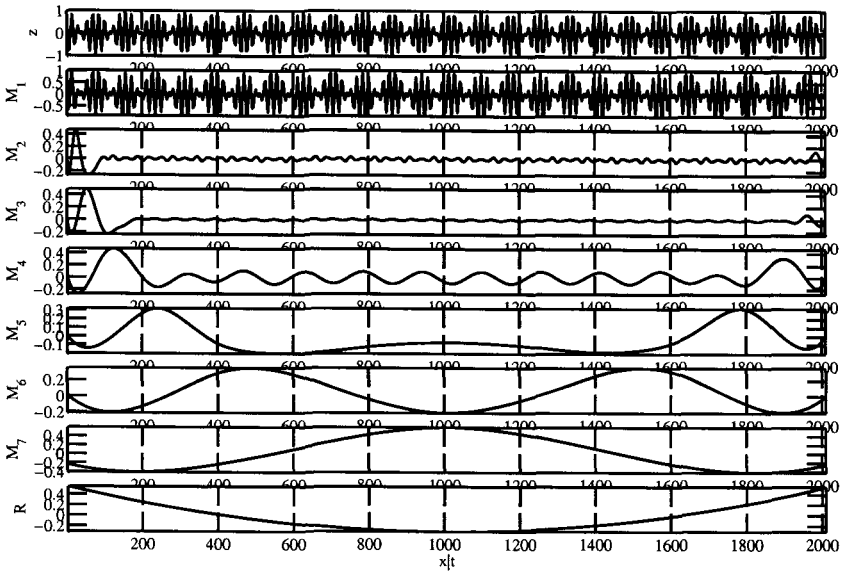

Figure 10.9: EMD processing of the signal shown in Fig. 10.8(a). The top panel is the original signal, M_1 to M_7, are the modes and R is the remainder.

pears whereas the Hilbert spectrum invariably shows low-frequency energy while the Fourier and wavelet spectra show energy only near the carrier frequency.

10.5. Summary

Analyzing nonlinear and nonstationary signals remains a very challenging task. Presently, most methods developed to deal with nonstationarity are based on the concept of Fourier decomposition; therefore, all the shortcomings associated with Fourier transformation are inherent in those methods also. The recent introduction of empirical mode decomposition by Huang et al. (1998, 1999) represents a fundamentally different approach for decomposing nonlinear and nonstationary signals. The associated spectral analysis (HHT) provides superior spatial (temporal) and wavenumber (frequency) resolution for handling nonstationarity and nonlinearity (section 10.2). The Hilbert spectrum also results in a considerably different interpretation of nonlinearity (frequency modulation). Applying the technique to the problems of wind-generated ocean waves, we found that the spectral function derived from the HHT is markedly different from those obtained by using the Fourier-based techniques. The difference in the resulting spectral functions is attributed to the interpretation of nonlinearity. The Fourier techniques decompose a nonlinear signal into sinusoidal harmonics; therefore, some of the spectral energy at the base frequency is distributed to the higher-frequency components. The HHT interprets nonlinearity in terms of frequency modulation, and the spectral energy remains in the neighborhood of the base frequency. This difference results in a considerably

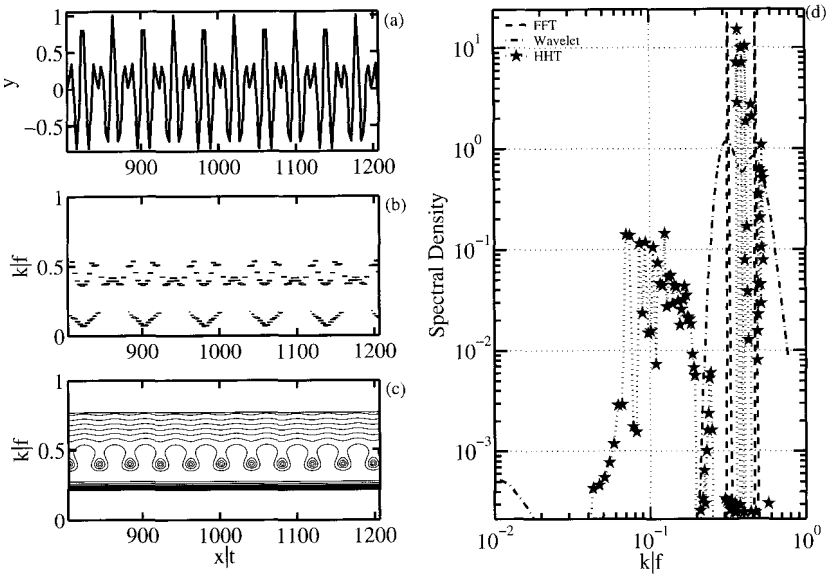

Figure 10.10: Same as Fig. 10.8, but the carrier period is $5\Delta t$, and the modulation period is $25\Delta t$, where Δt is the sampling time interval.

higher spectral energy at lower frequencies and sharper dropoff at higher frequencies in the Hilbert spectrum in comparison with the Fourier-based spectra. The mean frequency computed from the Hilbert spectrum is 13 to 21% lower than those derived from Fourier-based spectra. On the other hand, for the basic statistical measures such as the spectral bandwidth or spectral moments, the results computed from the Hilbert and Fourier spectra are similar, suggesting that the study of the statistical properties of ocean waves is probably not affected by using the Hilbert spectral technique. Finally, wave group structures in the time series of surface displacement represent low-frequency oscillations. When processing the results from Fourier analysis, however, one may interpret the wave group as the interaction of two wave components with a slight difference in their frequencies, and the spectral energy does not appear at the observed frequency of wave groups. The Hilbert analysis places the spectral energy of the wave group at the correct frequency band if it is distinct enough from the carrier frequency.

Acknowledgements

This work was supported by the Office of Naval Research (Naval Research Laboratory Program Elements N61153 and N62435, PAH, DWW, and JMK) and the NASA RTOP program on micro-scale ocean dynamics (NEH). This chapter is NRL contribution BC/7330-03-0002.

References

Bitner-Gregersen, E. M., and S. Gran, 1983: Local properties of sea waves derived from a wave record. *Appl. Ocean Res.*, **5**, 210–214.

Chapman, R. D., and F. M. Monaldo, 1991: The APL wave gauge system. Rep. S1R-91U-041, Applied Physics Laboratory, The Johns Hopkins University, Baltimore, MD, 25 pp.

Guillaume, D. W., 2002: A comparison of peak frequency-time plots produced with Hilbert and wavelet transforms. *Rev. Sci. Instrum.*, **73**, 98–101.

Huang, N. E., S. R. Long, C. C. Tung, Y. Yuan, and L. F. Bliven, 1983. A non-Gaussian statistical model for surface elevation of nonlinear random wave fields. *J. Geophys. Res.*, **85**, 7597–7606.

Huang, N. E., Z. Shen, S. R. Long, M. C. Wu, H. H. Shih, Q. Zheng, N.-C. Yen, C. C. Tung, and H. H. Liu, 1998: The empirical mode decomposition and the Hilbert spectrum for nonlinear and non-stationary time series analysis. *Proc. R. Soc. London, Ser. A*, **454**, 903–995.

Hwang, P. A., and D. W. Wang, 2004: Field measurements of duration limited growth of wind-generated ocean surface waves at young stage of development. *J. Phys. Oceanogr.*, **34**, 2316–2326.

Hwang, P. A., D. Xu, and J. Wu, 1989: Breaking of wind-generated waves: Measurements and characteristics. *J. Fluid Mech.*, **202**, 177–200.

Liu, P. C., 2000: Is the wind wave frequency spectrum outdated? *Ocean Eng.*, **27**, 577–588.

Longuet-Higgins, M. S., 1952: On the statistical distribution of the heights of sea waves. *J. Mar. Res.*, **11**, 245–266.

Longuet-Higgins, M. S., 1980: On the distribution of the heights of sea waves: Some effects of nonlinearity and finite band width. *J. Geophys. Res.*, **85**, 1519–1523.

Massel, S. R., 2001: Wavelet analysis for processing of ocean surface wave records. *Ocean Eng.*, **28**, 957-987.

Melville, W. K., 1983: Wave modulation and breakdown. *J. Fluid Mech.*, **128**, 489-506.

Shen, Z., and L. Mei, 1993: Equilibrium spectra of water waves forced by intermittent wind turbulence. *J. Phys. Oceanogr.*, **23**, 2019–2026.

Shen, Z., W. Wang, and L. Mei, 1994: Finestructure of wind waves analyzed with wavelet transform. *J. Phys. Oceanogr.*, **24**, 1085–1094.

Veltcheva, A. D., 2002: Wave and group transformation by a Hilbert spectrum. *Coast. Eng. J.*, **44**, 283–300.

Veltcheva, A. D., P. Cavaco, and C. Guedes Soares, 2003: Comparison of methods for calculation of the wave envelope. *Ocean Eng.*, **30**, 937–948.

Paul A. Hwang
Oceanographic Division, Naval Research Laboratory, Stennis Space Center, MS 39529, USA
paul.hwang@nrlssc.navy.mil

Norden E. Huang
Goddard Institute for Data Analysis, Code 614.2, NASA/Goddard Space Flight Center, Greenbelt, MD 20771, USA
norden.e.huang@nasa.gov

David W. Wang
Oceanographic Division, Naval Research Laboratory, Stennis Space Center, MS 39529, USA
david.wang@nrlssc.navy.mil

James M. Kaihatu
Oceanographic Division, Naval Research Laboratory, Stennis Space Center, MS 39529, USA
james.kaihatu@nrlssc.navy.mil